Research Article | Vol. 27, No. 13 | 24 Jun 2019 | OPTICS EXPRESS 19042
Optics EXPRESS

# Terahertz optical characteristics of two types of metamaterials for molecule sensing

YEEUN ROH,[1,2] SANG-HUN LEE,[1] BOYOUNG KANG,[3] JEONG WEON WU,[4] BYEONG-KWON JU,[2] AND MINAH SEO[1,5,*]

[1]*Sensor System Research Center, Korea Institute of Science and Technology (KIST), Seoul, 02792, South Korea*
[2]*Display and Nano system Laboratory, College of Engineering, Korea University, Seoul, 02841, South Korea*
[3]*Center for Advanced Meta-materials, Daejeon, 34103, South Korea*
[4]*Department of Physics, Ewha Womans University, Seoul, 03760, South Korea*
[5]*Division of Nano & Information Technology, KIST School, Korea University of Science and Technology, Seoul, 02792, South Korea*
**mseo@kist.re.kr*

**Abstract:** We investigate spectral responses of two different terahertz (THz) metamaterials of double split ring resonator (DSRR) and the nano slot resonator (NSR) for molecule sensing in low concentration. Two different resonant frequencies of DSRR can be controlled by polarization angle of incident THz beam. For comparison of THz optical characteristics, two NSRs were made as showing the same resonant frequencies as DSRR's multimode. The monosaccharide molecules of glucose and galactose were detected by these two types of metamaterials matching the resonant frequencies in various concentration. NSR shows higher sensitivity in very low concentration range rather than DSRR, although the behavior was easily saturated in terms of concentration. In contrast, DSRR can cover more broad concentration range with clear linearity especially under high quality factor mode in polarization of 67.5 degree due to the Fano resonance. THz field enhancement distributions were calculated to investigate sensing performance of both sensing chips in qualitative and quantitative manner.



## 1. Introduction

Terahertz (THz) time-domain spectroscopy [1,2] research has been explored in various areas encompassing fields such as security applications [3–5], biomedical or pharmaceutical imaging [6–9] and sensing for chemicals [10,11] since it enables to non-invasive, non-destructive and label-free detection of target materials. In particular, THz spectroscopy has drawn attention for new detection method of bio-materials because of energy level of biomolecular vibration including vibration, libration, tortion and rotation lying in THz range [12–17]. These distinctive characteristics of various molecules enable fingerprinting of biomolecules even for very similar molecule structure cases. During past decades, lots of biomolecules such as protein, DNA and carbohydrates have been studied using THz techniques in various ways [12,16–19]. Nevertheless, there are still challenges in biomolecular detection using optical sensing ways, because of its very low concentration in organisms and low absorption cross-section in the THz range. Metamaterials, resonant metallic structures created to realize nonexistent electromagnetic properties in nature, have been also widely researched for such sensing purposes. Those show fascinating characteristics including sensitivity enhancement depending on their geometry. The split ring resonator (SRR), especially, was used for molecular sensing [20] by monitoring resonant frequency shift. The frequency shift is caused by capacitance change related to refractive index of analytes inside the gap, where there is hotspot of induced electric field [21]. As another candidate, the nanostructured metallic slot induces huge absorption cross-section

#364688 https://doi.org/10.1364/OE.27.019042
Journal © 2019 Received 9 Apr 2019; revised 4 Jun 2019; accepted 4 Jun 2019; published 21 Jun 2019

Optics EXPRESS

enhancement by asymmetric amplification between electric and magnetic fields [22,23]. Thus sensitive detection of saccharides was possible by obtaining huge enhancement of absorption cross-section of detection target [22–25].

In this paper, we demonstrate THz molecular detection using metamaterial sensing chips, which are based on the DSRR and the NSR for selective detection of some analytes in low concentration. We used monosaccharides as the analytes which have very similar molecular formula. Glucose is the most important carbohydrate molecule because it is essential for metabolism including synthesizing structural polymers, oxidation for energy and storage. It also has an important role in human being for the diagnosis of diabetes by detecting the concentration of glucose in the blood. It has fingerprint frequency near 1.4 THz where we choose the DSRR's one resonance frequency and the resonance frequency of shorter NSR. Galactose, which is another sample of monosaccharides, has identical molecular formula and chemical structure except one orientation of the hydroxyl group (-OH) at 4th carbon compared to glucose. It shows weak absorption near 1.2 THz where also was fitted to another resonance of DSRR and resonance frequency of longer NSR. In spite of their molecular similarity, it was reported that the molecular vibrational modes lying in THz range are very distinguishable [17,25]. We first applied a metamaterial sensor of DSRR which has unusual resonance behavior that resonance frequency is tunable by polarization direction of incident waves on a single chip [26]. Thus it was exploited as dual mode sensing device for two molecules. The sensing performance was directly compared to the nano-slot based sensor with various sample concentrations. We also performed a finite element method (FEM) simulation to confirm the different THz optical behaviors between DSRR and NSR.

## 2. Materials and experiment setup

We obtained the transmission spectra using THz time-domain spectroscopy system from 0.5 to 2.0 THz range. Basically, Ti:sapphire femtosecond laser with center wavelength of 800 nm and repetition rate of 80 MHz was used to drive the THz system. The femtosecond laser beam was split into pump and probe beams. The pump beam was incident on the photoconductive antenna to generate THz pulse. Then generated THz pulse was collimated by parabolic mirrors and focused onto the metamaterial using the polymethylpentene (TPX) lens. The transmitted THz signal through the sample was measured by electro-optic sampling technique based on ZnTe crystal using time delay between the probe beam and the generated THz pulse. This system was enclosed with purged air to avoid unwanted absorption by water vapor. The THz spectrum was obtained by Fast Fourier Transform (FFT) from time-domain waveform. The transmittance of the sensing surface of metamaterial is defined as $T(\omega) = \left|E_{sample}(\omega)\right|^2 \Big/ \left|E_{Si}(\omega)\right|^2$ where $E_{Si}(\omega)$ and $E_{sample}(\omega)$ are amplitudes of transmitted electric field through the metamaterial and Si substrate attached on a metallic sample holder with a square hole of 1.6 mm × 1.6 mm, respectively. Incident THz polarization was occasionally changed, up to the metamaterial type.

The metamaterial sensor consists of DSRR array where each elementary DSRR has an inner radius of 14 μm and outer radius of 18 μm as shown in Fig. 1(a). Two DSRRs with different rotation angles, which gaps are opened along *x*-axis (0°) and the axis along 135° direction, were alternatively aligned at a sensing surface for polarization-dependent multi resonance behavior [26]. Thickness of gold pattern of DSRR is 200 nm with 10 nm of titanium adhesion layer, which can be handled as a perfect electric conductor at reliable THz regime, because of the thickness higher than the skin depth. The transmittance spectra of DSRR were observed with the different polarization direction of incident THz waves. The spectra by incident polarization angle of 0° and 67.5° have respective resonance features at 1.4 THz and 1.2 THz, as shown in Fig. 1(b). The reason why we choose these two frequencies is that 1.2 THz and 1.4 THz show fingerprint feature for galactose and glucose, respectively. The sharp resonance on 1.2 THz is induced by the Fano resonance from symmetric breaking

Optics EXPRESS

between resonances of adjacent DSRR unit cells. Then the glucose and galactose were applied onto the DSRR metamaterial sensing surface by the conventional drop-and-dry method of liquid sample [25]. The monosaccharide molecules of galactose and glucose were purchased from Sigma-Aldrich Co. and prepared as aqueous solutions by dissolving in deionized water at room temperature. The aqueous solutions of 1 μg/μL to 5 μg/μL were individually dropped on the metamaterial using pipettes and dried within 10 minutes to remove the absorption effect of water in THz range, as depicted in Fig. 1(c). We also designed the nano slot resonators (NSRs) for identical resonances to two cases of different polarization angles for DSRRs, as described above. The NSRs for resonant frequencies of 1.2 THz and 1.4 THz have lengths of 48.9 μm and 40 μm, respectively. Each slot is separated by 40 μm in the transverse direction and 10 μm in the longitudinal direction. Incident THz polarization was perpendicular to the long direction of the NSR. Both metamaterials of DSRRs and NSRs can be fabricated by conventional photolithography method on high resistivity silicon wafers.

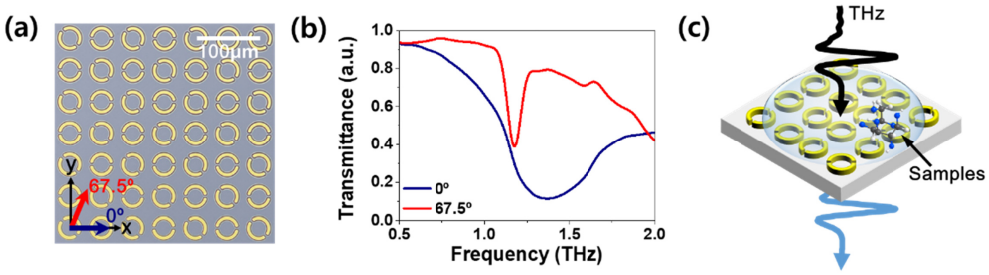


Fig. 1. (a) Microscope picture of DSRR metamaterial. (b) THz transmittances of DSRR are shown for different polarization angles of incident THz field. Resonances are shown at 1.2THz for polarization angle 67.5° and 1.4THz for polarization angle 0°. (c) A schematic of THz transmission through DSRR covered with monosaccharide sample droplet.

## 3. Result and discussion

The transmittance spectra for glucose and galactose of 3 μg/μL on top of DSRR's surface are shown in Fig. 2. The transmittances of glucose and galactose are plotted by green curves in Figs. 2(a) and 2(b), and blue curves in Figs. 2(c) and 2(d), respectively, with certain rotation in azimuthal angle of DSRR for resonance of 1.2 and 1.4 THz. The spectra for angle of 0° are shown in Figs. 2(a) and 2(c) and the spectra for angle of 67.5° are shown in Figs. 2(b) and 2(d). All transmittance spectra with samples are shifted toward a lower frequency regime with regard to the refractive index of samples. The gaps in DSRR behave like capacitors in the LC circuit which have resonant frequencies depending on the optical impedance or the refractive index of surrounding materials. Thus, it can be possible to detect sensitively and determine the refractive index of analyte by monitoring the resonance frequency shift.

Optics EXPRESS

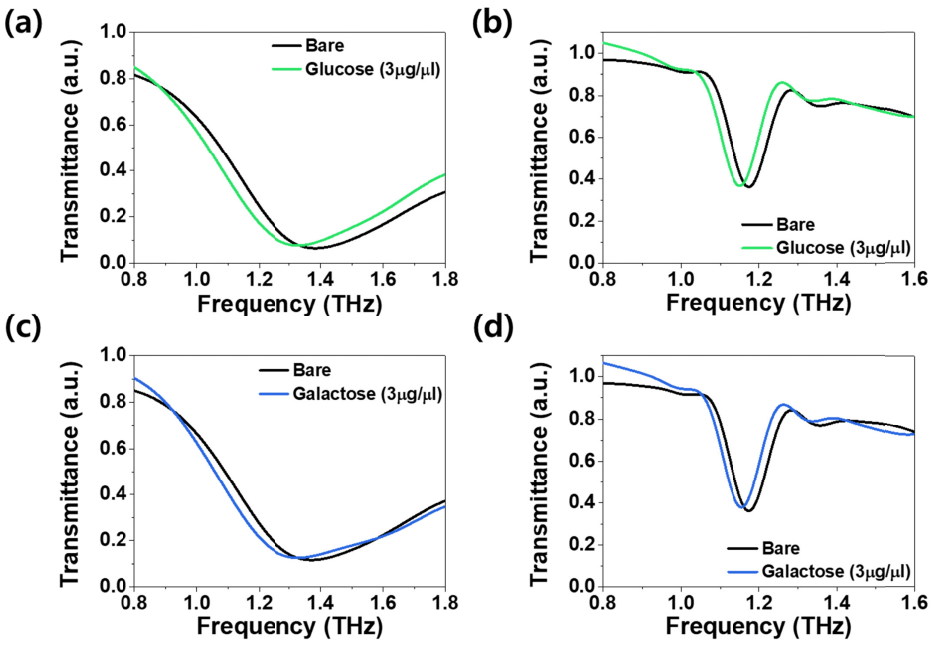


Fig. 2. Normalized THz transmittance spectra of DSRR with (a), (c) polarization angle of 0° and (b), (d) polarization angle of 67.5° with glucose and galactose of 3 μg/μL. Green and blue lines denote the measured spectra for glucose and galactose, respectively.

We progressively increased the concentration of samples from 0.1 μg/μL to 5 μg/μL and obtained the resonant frequency shifts ($-\Delta f/f_0 = -(f_{sample} - f_0)/f_0$) as plotted in Fig. 3. The trends of the frequency shift were fitted using Michelson-Menten function represented as $-\Delta f/f_0 = V_{\max} x/(K_m + x)$ [27], where $V_{\max}$ is a maximum of frequency change, and $K_m$ is a slope of a curve depicting sensitivity. The resonance is almost linearly redshifted in terms of concentration in both 1.2 THz and 1.4 THz cases as represented in Figs. 3(a) and 3(b). In particular, the resonance shift of the sharp Fano resonance at 1.2 THz strictly represents a linear trend with much less deviation than other cases as shown in Fig. 3(a). Both monosaccharide analytes show a larger frequency shift at 1.4 THz than 1.2 THz. Furthermore, the resonance frequency shifts for glucose are always larger than that of galactose even if the resonant frequency is changed by tuning the polarization angle. The ring oscillator has the resonance frequency shift, $\Delta f \sim f_0/n_{eff}$, where $f_0$ is the fundamental resonance frequency without the sample, and $n_{eff}$ is the effective complex refractive index of the surrounding [28]. The response difference between two frequencies is based on the combination of refractive indices of analytes and the fundamental resonance frequency of the metamaterial [29]. Glucose has a strong absorption feature at 1.4 THz, while galactose does not have a noticeable absorption mode in the measured frequency range. This clear spectral feature only for glucose may affect different concentration dependence in frequency shift especially at 1.4 THz contrary to 1.2 THz where both samples have similar refractive indices [25,29]. Galactose has weak absorption at 1.2 THz, which is not dominant for the frequency shift rather than refractive index difference. Such distinguishable slopes related with different refractive properties for glucose and galactose at 1.4 THz allows us to selectively detect different molecules in low concentration level, with just simple rotating of the azimuthal angle of the sensing chip.

We performed the same experimental process with another metamaterial, NSRs, which has negative metal patterns to compare the THz optical response with DSRR. The frequency shifts, $-\Delta f/f_0$, with NSRs are plotted in Figs. 3(c) and 3(d). The resonances are also

Optics EXPRESS

redshifted with glucose and galactose monotonically. The frequency shifts of NSR are larger than those of DSRR in very low concentration level, although the shift is gradually saturated on both NSRs in relatively high concentration level. It is noted that, at 1.4 THz (Fig. 3(d)), glucose shows a larger shift than galactose, which is similar behavior to the result with DSRR, owing to the glucose absorption feature at this frequency. Finally, it can be concluded that NSR is sensitive in very low concentration level, even though it is readily saturated. Meanwhile, DSRR can cover broader concentration range with well-defined linearity. Especially high quality (Q)-factor from the DSRR owing to the Fano resonance can contribute to such a clearly linear sensing response, which is very important parameter as a figure-of-merit of molecule sensors. The linear behavior with different slope also can be applied to the selective molecule sensing for even such similar chemical structures.

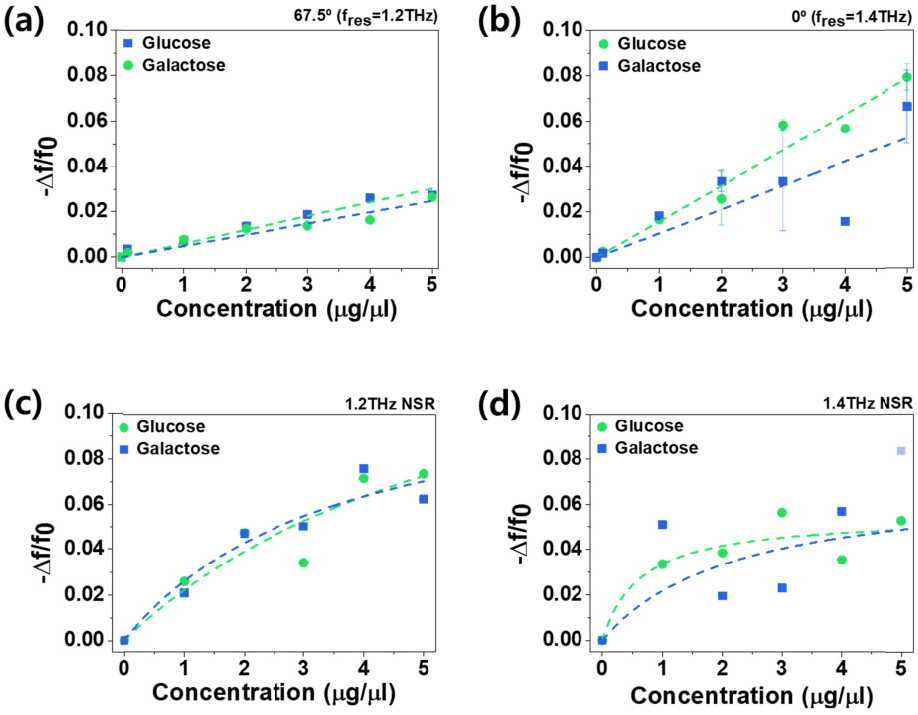


Fig. 3. The resonant frequency shifts extracted from measurements with DSRR under polarization angle of (a) 67.5° and (b) 0° are plotted showing different fundamental resonance frequencies. The resonant frequency shifts from measurements with NSR of resonance at (c) 1.2 THz and (d) 1.4THz are shown.

To confirm the results, we performed finite element method (FEM) simulation using COMSOL Multiphysics software. The THz electric field is normally incident on the surface of NSR while the electric field polarized as 67.5° is incident on the DSRR in calculation to show the same resonance frequency of 1.2 THz. The electric field of two elementary DSRRs is shown in Fig. 4(a). The calculated region was cropped and enlarged from the whole structure as described in the inset. Since the DSRR is composed of positive patterns on the substrate, the field enhancement is on the metal boundary near the gap as shown in Fig. 4(a). On the contrary to this, the field enhancement takes place inside the gap between the metals in the NSR as shown in Fig. 4(b). The amplitudes of the electric field along the dashed line across the hotspot of the DSRR and the NSR structures are depicted in Figs. 4(c) and 4(d), respectively. The width of metal rings of DSRR is $w = 4$ μm while the gap size of NSR is $w =$ 500 nm. The localized field amplitude inside the gap of NSR is much more intense than that of DSRR, because the gap size of the NSR is much narrower almost one order than the split

Optics EXPRESS

ring width, which were well-confirmed with previous works [30]. It can be related to the measured results that NSR was more sensitive to the analyte samples in very low concentration regime. Meanwhile, NSR can be easily saturated where the molecular concentration increases as compare to DSRR.

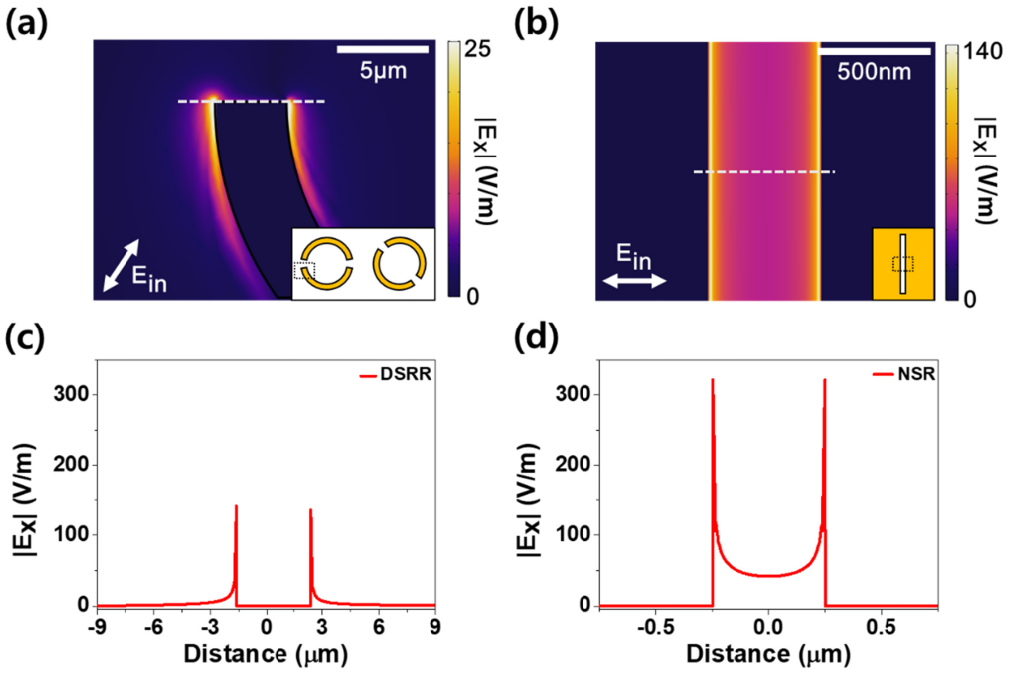


Fig. 4. The calculated electric field distribution ($|E_x|$) of (a) DSRR and (b) NSR at the resonance frequency, 1.2 THz. The amplitude of electric field along the dashed lines are depicted in (c) and (d).

## 4. Conclusion

In conclusion, we demonstrated molecule sensing platforms using two different types of metamaterials including DSRR and NSR patterns in THz spectroscopy. We compared the sensing characteristics of two metamaterials, which have multi-resonances at 1.2 THz and 1.4 THz. In this experiment, two monosaccharide molecules of glucose and galactose were used as samples since they have very similar chemical structures. The resonant frequency shifts for dropped samples in low concentrations were obtained in accordance with the sensitivity of the metamaterials. We found that NSR is more sensitive at very low concentration regime which is related to the higher field enhancement factors from the narrower gap size, however, it is readily saturated in terms of the concentration. There is clear trade-off between field enhancement and sensitivity increase by narrowing down the gap size, and available concentration range limited by the low Q-factor. The saturation behavior is very critical, bothering the validity in expanded detection range. Even though the sensitivity is a little lower than NSR, in the meanwhile, the DSRR can guarantee wider detectable concentration range with clear linearity originated from the sharp Fano resonance. Further studies with such metamaterial sensing chips with narrower gap size to increase the sensitivity, maintaining higher Q-factor, will allow us to realize super highly sensitive and selective THz molecule sensing, to make non-invasive detection ultimately possible.

Optics EXPRESS

## Funding

National Research Foundation of Korea (NRF) (Global Frontier Program CAMM-2014M3A6B3063700, 2019M3A6B3030638, and 2017R1E1A1A01075394); KIST intramural grants (2E29490 and 2V06780).

## Acknowledgments

The authors acknowledge valuable discussion on simulation with Dr. Dukhyung Lee and Dr. Seo Joo Lee.

## References

1. M. Tonouchi, "Cutting-edge terahertz technology," Nat. Photonics **1**(2), 97–105 (2007).
2. P. U. Jepsen, D. G. Cooke, and M. Koch, "Terahertz spectroscopy and imaging - Modern techniques and applications," Laser Photonics Rev. **5**(1), 124–166 (2011).
3. M. C. Kemp, P. F. Taday, B. E. Cole, J. A. Cluff, A. J. Fitzgerald, and W. R. Tribe, "Security applications of terahertz technology," Terahertz Mil. Secur. Appl. **5070**, 44–52 (2003).
4. J. F. Federici, B. Schulkin, F. Huang, D. Gary, R. Barat, F. Oliveira, and D. Zimdars, "THz imaging and sensing for security applications - Explosives, weapons and drugs," Semicond. Sci. Technol. **20**(7), S266–S280 (2005).
5. H. B. Liu, H. Zhong, N. Karpowicz, Y. Chen, and X. C. Zhang, "Terahertz spectroscopy and imaging for defense and security applications," Proc. IEEE **95**(8), 1514–1527 (2007).
6. K. Ajito and Y. Ueno, "THz chemical imaging for biological applications," IEEE Trans. Terahertz Sci. Technol. **1**(1), 293–300 (2011).
7. S. J. Oh, S. H. Kim, K. Jeong, Y. Park, Y. M. Huh, J. H. Son, and J. S. Suh, "Measurement depth enhancement in terahertz imaging of biological tissues," Opt. Express **21**(18), 21299–21305 (2013).
8. X. Yang, X. Zhao, K. Yang, Y. Liu, Y. Liu, W. Fu, and Y. Luo, "Biomedical Applications of Terahertz Spectroscopy and Imaging," Trends Biotechnol. **34**(10), 810–824 (2016).
9. G. G. Hernandez-Cardoso, S. C. Rojas-Landeros, M. Alfaro-Gomez, A. I. Hernandez-Serrano, I. Salas-Gutierrez, E. Lemus-Bedolla, A. R. Castillo-Guzman, H. L. Lopez-Lemus, and E. Castro-Camus, "Terahertz imaging for early screening of diabetic foot syndrome: A proof of concept," Sci. Rep. **7**(1), 42124 (2017).
10. H. Zhong, A. Redo-Sanchez, and X.-C. Zhang, "Identification and classification of chemicals using terahertz reflective spectroscopic focal-plane imaging system," Opt. Express **14**(20), 9130–9141 (2006).
11. R. Kumar, A. Kumar, V. Deval, A. Gupta, P. Tandon, P. S. Patil, P. Deshmukh, D. Chaturvedi, and J. G. Watve, "Molecular structure, spectroscopic (FT-IR, FT Raman, UV, NMR and THz) investigation and hyperpolarizability studies of 3-(2-Chloro-6-fluorophenyl)-1-(2-thienyl) prop-2-en-1-one," J. Mol. Struct. **1129**, 292–304 (2017).
12. B. M. Fischer, M. Walther, and P. Jepsen, "Far-infrared vibrational modes of DNA components studied by terahertz time-domain spectroscopy," Phys. Med. Biol. **47**(21), 3807–3814 (2002).
13. M. Nagel, F. Richter, P. Haring-Bolívar, and H. Kurz, "A functionalized THz sensor for marker-free DNA analysis," Phys. Med. Biol. **48**(22), 3625–3636 (2003).
14. K. Tsukada, M. Tonouchi, Y. Kondo, T. Kiwa, I. Kawayama, and Y. Minami, "Terahertz chemical microscope for label-free detection of protein complex," Appl. Phys. Lett. **96**(21), 211114 (2010).
15. F. Wang, D. Zhao, H. Dong, L. Jiang, Y. Liu, and S. Li, "Terahertz spectra of DNA nucleobase crystals: A joint experimental and computational study," Spectrochim. Acta A Mol. Biomol. Spectrosc. **179**, 255–260 (2017).
16. R. G. Zhbankov, S. P. Firsov, D. D. Grinshpan, J. Baran, M. K. Marchewka, and H. Ratajczak, "Vibrational spectra and noncovalent interactions of carbohydrates molecules," J. Mol. Struct. **645**(1), 9–16 (2003).
17. P. C. Upadhya, Y. C. Shen, A. G. Davies, and E. H. Linfield, "Far-infrared vibrational modes of polycrystalline saccharides," Vib. Spectrosc. **35**(1-2), 139–143 (2004).
18. M. Walther, P. Plochocka, B. Fischer, H. Helm, and P. Uhd Jepsen, "Collective vibrational modes in biological molecules investigated by terahertz time-domain spectroscopy," Biopolymers **67**(4-5), 310–313 (2002).
19. T. R. Globus, D. L. Woolard, T. Khromova, T. W. Crowe, M. Bykhovskaia, B. L. Gelmont, J. Hesler, and A. C. Samuels, "THz-Spectroscopy of Biological Molecules," J. Biol. Phys. **29**(2-3), 89–100 (2003).
20. R. Singh, I. A. I. Al-Naib, M. Koch, and W. Zhang, "Sharp Fano resonances in THz metamaterials," Opt. Express **19**(7), 6312–6319 (2011).
21. T. Driscoll, G. O. Andreev, D. N. Basov, S. Palit, S. Y. Cho, N. M. Jokerst, and D. R. Smith, "Tuned permeability in terahertz split-ring resonators for devices and sensors," Appl. Phys. Lett. **91**(6), 062511 (2007).
22. M. A. Seo, H. R. Park, S. M. Koo, D. J. Park, J. H. Kang, O. K. Suwal, S. S. Choi, P. C. M. Planken, G. S. Park, N. K. Park, Q. H. Park, and D. S. Kim, "Terahertz field enhancement by a metallic nano slit operating beyond the skin-depth limit," Nat. Photonics **3**(3), 152–156 (2009).
23. H. R. Park, K. J. Ahn, S. Han, Y.-M. Bahk, N. Park, and D. S. Kim, "Colossal absorption of molecules inside single terahertz nanoantennas," Nano Lett. **13**(4), 1782–1786 (2013).
24. J.-H. Kang, D.-S. Kim, and M. Seo, "Terahertz wave interaction with metallic nanostructures," Nanophotonics **7**(5), 763–793 (2018).

Optics EXPRESS


25. D. K. Lee, J. H. Kang, J. S. Lee, H. S. Kim, C. Kim, J. H. Kim, T. Lee, J. H. Son, Q. H. Park, and M. Seo, "Highly sensitive and selective sugar detection by terahertz nano-antennas," Sci. Rep. **5**(1), 15459 (2015).
26. B. Kang, E. Choi, H.-H. Lee, E. S. Kim, J. H. Woo, J. Kim, T. Y. Hong, J. H. Kim, and J. W. Wu, "Polarization angle control of coherent coupling in metamaterial superlattice for closed mode excitation," Opt. Express **18**(11), 11552–11561 (2010).
27. L. B. Sheiner and S. L. Beal, "Evaluation of methods for estimating population pharmacokinetic parameters. II. Biexponential model and experimental pharmacokinetic data," J. Pharmacokinet. Biopharm. **9**(5), 635–651 (1981).
28. S. J. Park, J. T. Hong, S. J. Choi, H. S. Kim, W. K. Park, S. T. Han, J. Y. Park, S. Lee, D. S. Kim, and Y. H. Ahn, "Detection of microorganisms using terahertz metamaterials," Sci. Rep. **4**(1), 4988 (2015).
29. T. Zhang, A. Tao, and S. Yan, "Terahertz Time-Domain Spectroscopy of Crystalline Glucose and Galactose," Int. Conf. Bioinform. Biomed. Eng. **978**, 1146–1149 (2008).
30. G. Choi, Y. M. Bahk, T. Kang, Y. Lee, B. H. Son, Y. H. Ahn, M. Seo, and D. S. Kim, "Terahertz Nanoprobing of Semiconductor Surface Dynamics," Nano Lett. **17**(10), 6397–6401 (2017).